Proceedings of the ASME 2010 3rd Joint US-European Fluids Engineering Summer Meeting and 8th International Conference on Nanochannels, Microchannels, and Minichannels
FEDSM-ICNMM2010
August 1-5, 2010, Montreal, Canada

FEDSM-ICNMM2010-30970

MODELING AND EXPERIMENTS OF A RESONANT SONOCHEMICAL REACTOR

Yi-Chun Wang
Department of Mechanical Engineering,
National Cheng Kung University,
Tainan, Taiwan 70101

Ming-Chung Yao
Department of Mechanical Engineering,
National Cheng Kung University,
Tainan, Taiwan 70101

ABSTRACT

This work aims at analyzing and realizing a horn-type sonochemical reactor which can be operated in a very low ultrasonic power density but results in a large volume of cavitation zones. The sonoreactor contains three main components, namely a Langevin-type piezoelectric transducer (20 kHz), a metal horn, and a circular cylindrical sonicated cell filled with tap water. In order to diminish the generation of cavitation bubbles near the horn-tip, an enlarged cone-shaped horn is designed to reduce the ultrasonic intensity at the irradiating surface and to get better distribution of energy in the sonicated cell. It is demonstrated both numerically and experimentally that the cell geometry and the horn position have prominent effects on the pressure distribution of the ultrasound in the cell. With appropriate choices of these parameters, the whole reactor works at a resonant state. Several acoustic resonance modes observed in the simulation are realized experimentally and used for generating a large volume of cavitation field.

INTRODUCTION

Sonochemical effects of high intensity ultrasound come mainly from acoustic cavitation. Cavitation bubble collapse in liquid can be so violent that very high local pressure and temperature, combined with extraordinarily cooling, provide a unique environment for driving chemical reactions under extreme conditions. In a standard immersed-type sonochemical reactor, an ultrasonic horn with shrinking cross-sectional area is used to amplify the intensity of the ultrasound generated from a piezoelectric transducer. As a result, the cavitation bubbles are first formed very near the horn tip. The presence of bubbles causes severe attenuation of irradiating ultrasound. The fast decrease in ultrasonic intensity implies that cavitation activity is limited in the vicinity of the horn, causing poor efficiency of energy conversion for sonochemical effects, severe erosion of the sonicator surface, contamination of the reaction mixture, and degeneration of the system performance. Indeed, Gogate and Pandit et al. [1] found that, due to the limited cavitating region, the energy efficiency and cavitation yield of the horn-type sonochemical reactor are much lower than those of other ultrasonic equipments with multiple transducers, such as an ultrasonic bath and dual- or triple-frequency flow cells; the ultrasonic energy is dissipated mainly in the bulk volume of the liquid in the reactor without contributions to the cavitation activity. This limitation also makes the horn-type reactor unfavourable for large-scale industrial applications.

The typical radiating ultrasound intensity of the horn-type reactor (defined as the electrical power input to the transducer divided by the radiating surface area of the horn) is of the order of 100 W/cm^2. The liquid volume in the sonicated cell, on the

NOMENCLATURE

a	Mass damping parameter (1/s)
b	Stiffness damping parameter (s)
$\mathbf{C}$	Damping matrix (kg/s)
$\mathbf{K}$	Stiffness matrix (kg/s^2)
f	Driving frequency of the transducer (1/s)
f_r	Resonance frequency (1/s)
H	Liquid height in the cell (mm)
h	Distance from the horn tip to cell bottom (mm)
I_e	Amplitude of electrical current into transducer (mA)
$\mathbf{M}$	Mass matrix (kg)
P_e	Electrical power input to transducer (W)
R	Radius of cell (mm)
r	Circular cylindrical radial direction (mm)
V_e	Voltage amplitude for driving piezoelectric transducer (Volt)
z	Circular cylindrical axis direction (mm)

Special characters

α	Attenuation coefficient of ultrasound (Np/m)

other hand, is relatively small. Therefore, a cooling system is a must for the temperature control of an ultrasonic horn reactor under continuous operations. In this work, we will demonstrate that a resonant horn-type reactor can be achieved so that a very low irradiating intensity (of the order of 0.1 W/cm^2) can cause a large volume of cavitation zones. The specific power density in the sonicated cell (defined as the electrical power per unit liquid volume) is so small (about 0.001 W/cm^3) that cooling is not necessary.

The correlation of the modal sound fields in a cylindrical cell with sonochemiluminescent and sonochemical reactions had been demonstrated by Birkin et al. [2,3]. The cell was constructed using a Perspex cylinder and a stainless plate for the bottom base. A sandwich transducer was attached on the base and used for generating sound field in the cell. By varying the driving frequency of the transducer, various acoustic resonant modes (standing wave patterns) predicted theoretically could be excited experimentally. It was shown that a large volume of cavitation action can be produced if the driving frequency and the transducer efficiency are tuned so that the sound fields generated by the transducer and by the reverberation from the vessel boundaries are summed appropriately to form a resonant acoustic mode in the cell.

Recently Klíma et al. [4] applied the above concept to a 20 kHz horn-type sonochemical reactor. Based on a finite elements analysis, they found an optimal cell geometry so that a resonant sound field occurred in the cell. The acoustic intensity reached very high values in two areas in the cell, one around the tip of the horn and the other located far away from the horn. The locations of these high intensity areas were qualitatively in agreement with the experimental observation of cavitating zones. There are two deficiencies in the work of Klíma et al. [4]. First, their numerical model does not incorporate any attenuation of the ultrasound. Therefore, the absolute value of the maximum intensity at the resonant state should theoretically be infinitive. The maximum value obtained numerically depends directly on the mesh density of grids. Second, in their model, only the acoustics of the liquid volume was considered. The vibration motion of the horn was treated as a boundary condition of a harmonic pressure with constant amplitude. Interactions between the liquid and the cell boundaries were also neglected. In practice, the horn is directly immersed in the cell. Therefore, the performance (resonant frequency, vibration amplitude, and efficiency) of the transducer must be affected by the physical states of the sonicated liquid (acoustic impedance, sound field, and cavitation). Therefore, to design an efficient resonant sonochemical reactor, it is necessary both numerically and experimentally to couple the transducer and sonicated liquid cell together.

In the present work, a finite elements model (FEM), which combines piezoelectric, structural, and acoustic modules, is used for analyzing the whole system. Effects of structural damping and ultrasound attenuation are also included in the model. Experimental measurements show that the FEM model is quite accurate for predicting the resonance frequency and vibration amplitude of the ultrasonic transducer. Both computations and experiments show that the resonance modes of the system are very sensitive to the cell geometry. Several modes presented in the simulation are realized experimentally by visualization of the cavitating fields in the cell.

REACTOR DESIGN

The reactor contains three main parts, namely a piezoelectric transducer, a metal horn, and a sonicated cell, as illustrated in Figure 1. The piezoelectric transducer used in this work is a 20 kHz Langevin-type ultrasonic transducer (Sunnytec Electronics Co., Ltd.) consisting of four piezoelectric PZT discs sandwiched between two metal masses (steel and aluminum). The assembly is designed so that the free end faces of the transducer have a maximum vibration displacement at the frequency of operation. The transducer has a diameter of 50 mm and a length of 107 mm with a maximum rating power of 1000 W.

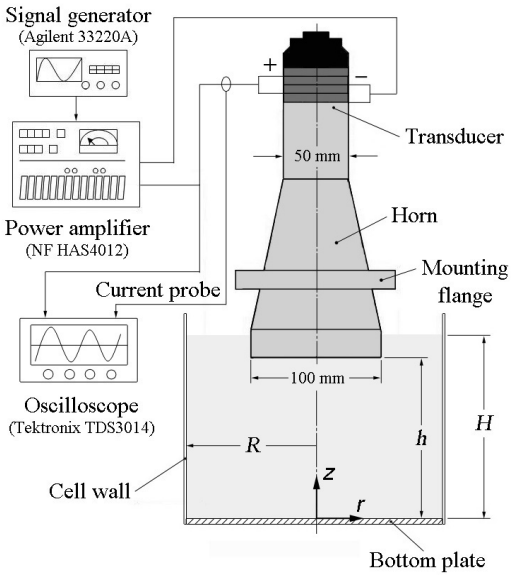

Figure 1 Schematic and experimental setup of the horn-type sonochemical reactor.

The vibration amplitude of the piezoelectric transducer is normally so small that the intensity of the ultrasound attainable by direct coupling of the transducer to the cell is not large enough to cause cavitation. Therefore, in most commercial sonochemical reactors, a metal horn with shrinking cross-sectional area is designed to amplify the vibration of the transducer. In this work, we take a reverse thinking: since the high intensity (or cavitating) areas in the cell need to be avoided to be a result of direct ultrasound irradiation from the horn tip but a sum of the radiation from the source and the reverberation from the cell boundaries, the energy density at the horn tip should be small enough so that cavitation will not occur therein to cause severe scattering and attenuation of the sound

propagation and to ruin the resonance of the cell. Therefore, the horn design in the present work adopts a circular enlarged cone shape to efficiently transfer the ultrasonic power from the transducer and at the same time to reduce the intensity irradiated by the horn tip. A mounting flange is designed on the horn for screw fixing of the transducer. The vertical position of the horn can be adjusted accurately by a precision ball-screw. The location of the flange must be carefully determined to minimize leakage of the ultrasonic energy. A FEM simulation is employed to design the horn as demonstrated later.

The cell containing the sonicated liquid (untreated tap water) is a home-made thin-wall circular vessel. The side wall of the cell is made of PC (poly-carbonate) with 0.5 mm in thickness glued on the edge of a 10 mm-thick aluminum circular plate. The diameter of the cell can be precisely controlled by choosing the diameter of the bottom plate. The geometry and configuration of the whole system are as represented in Figure 1, in which R is the radius of the cell, H is the height of the water, and h is the distance from the horn tip to the cell bottom. It will be shown that only some particular combinations of the cell geometry can generate resonant acoustic modes in the cell.

SIMULATIONS AND EXPERIMENTS OF ULTRASONIC TRANSDUCER AND HORN

For efficiently transferring the ultrasonic energy, the resonant frequency (in the axial compression mode) of the horn should match that of the transducer and the horn should be designed such that the interface between the horn and the transducer is located at a displacement antinode (or a stress nodal point). The combining structures of the transducer and horn are analyzed numerically using COMSOL Multiphysics™ finite elements software. The simulation of the transducer requires the solution of the partial differential equations for piezoelectric materials, in which the mechanical displacement is coupled with the electric potential. The elasticity matrix, piezoelectric matrix, and the relative permittivity matrix of the piezoelectric discs are set according to the material properties of PZT-4. Axisymmetric calculations are performed due to the geometric symmetry of the configuration. The boundary conditions for all the surfaces in contact with air are set as traction-free. In experiments the water cell is placed directly on an optical table and, therefore, the outside surface of the cell bottom can not be traction-free. However, most of the acoustic energy irradiating on the bottom plate are reflected back to the cell due to a large difference in the acoustic impedances of water and aluminum. The boundary condition of the cell bottom has a minor effect on the acoustic field in the cell. Indeed, we have set both traction-free and fixed boundary conditions at the outer surface of the bottom plate and found no quantitative difference. The computational domain is discretized by choosing triangular Lagrange-quadratic elements. Grid-independence test is performed by continuously refining the mesh. The total number of elements used in the simulation is 4147. Computational results are shown in Figure 2. It is evident from Figure 2(a) that the first longitudinal compression mode is located at 19.89 kHz, matching well with to the operation frequency of the transducer. As shown in Figure 2(b), a maximum displacement occurs at the junction surface of the horn and transducer. The displacement at the edge of the mounting flange is very small, allowing the horn to be fixed therein with minimum energy leakage. It should be noted that the displacement amplitude shown in Figure 2(a) is unrealistic because structural damping is not included yet. Under this situation the difference of the phase angles between the applied voltage and the resulting electrical current is always $\pi/2$. In other words, there is no net electrical power input to the transducer.

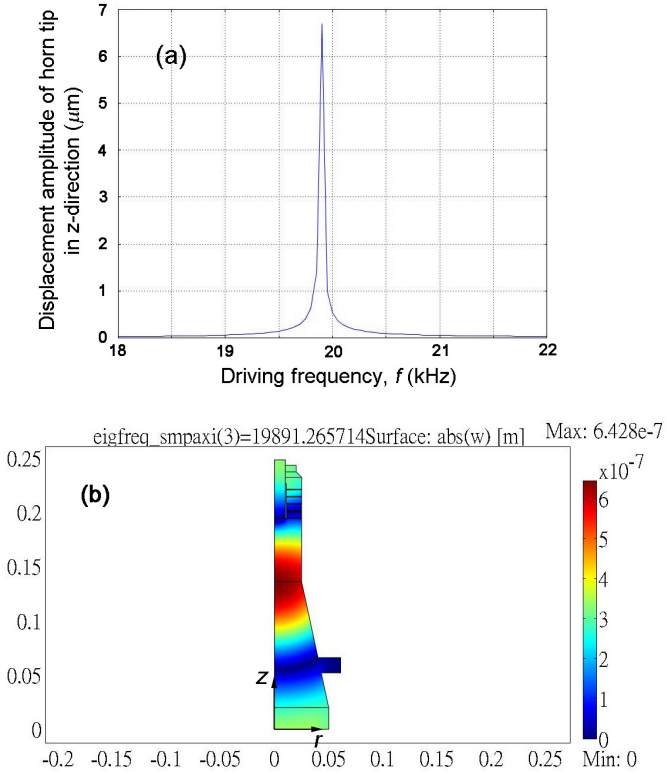

Figure 2 Simulation results of the transducer-horn structure: (a) variation of the maximum displacement amplitude (at the interface of the transducer and horn) with driving frequency (b) displacement amplitude in z-direction at the resonance frequency of 19.89 kHz. No structural damping included.

To predict the vibration and electrical power more accurately, a Rayleigh-damping model is incorporated into the FEM simulations. In this model the damping matrix is assumed to be a linear combination of the mass and stiffness matrices:

$$\mathbf{C} = a\mathbf{M} + b\mathbf{K} \tag{1}$$

where $\mathbf{C}$ is the damping matrix, $\mathbf{M}$ and $\mathbf{K}$ are finite element mass and stiffness matrices, a and b are mass and stiffness damping parameters respectively and need to be determined

according to the experimental damping ratios of the displacement at the selected resonance frequencies [5]. The accuracy of the FEM simulations is examined by comparing the numerical results with the experimental measurements at the first resonance frequency in the air (without coupling with the water cell). The amplitude of the driving voltage to the transducer in both the simulation and the experiment is set as V_e=50 V. Figure 3 illustrates a comparison of the variations of the electrical power and the displacement amplitude at the top surface of the transducer around the resonance frequency. The electrical powers are calculated by integrating the product of the electrical current and driving voltage over one period. Experimentally (referred to Figure 1), the electrical current is measured by a current probe (Tektronix TCP202) and is recorded with a digital oscilloscope (Tektronix TDS 3014). The displacement amplitudes are measured using a CCD laser displacement sensor (LK-G30, Keyence, 50 kHz, resolution 0.05 μm). Displacements at other locations are also compared in Table 1. The matching between the simulations and experiments is reasonably good.

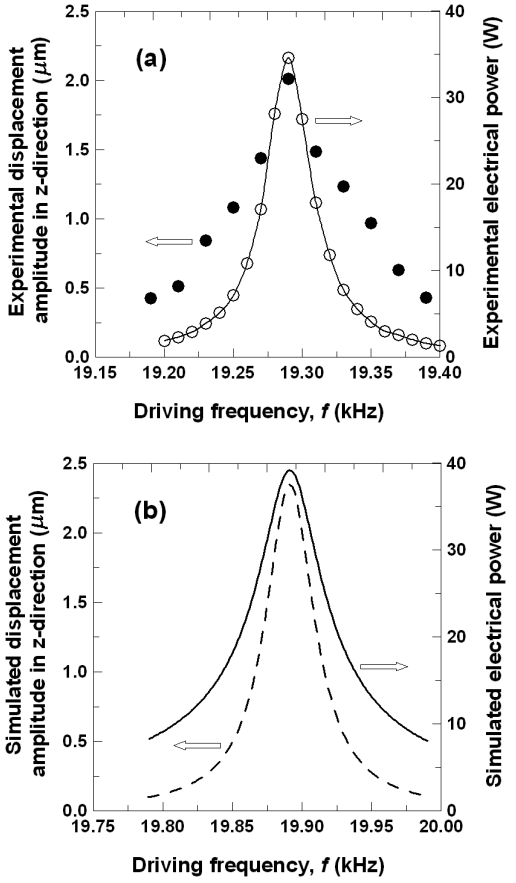

Figure 3 Variations of the displacement amplitude of transducer top surface and the input electrical power as functions of driving frequency from (a) experiments (b) simulations. (V_e=50 V)

EFFECTS OF CELL GEOMETRY ON RESONANCE FREQUENCY AT LOW ULTRASONIC INTENSITY

After validating the FEM model used for analyzing the vibrations of the transducer and the horn, we now couple the water cell to the horn in the model to form a complete design tool for the sonochemical system. Distribution of the acoustic pressure in the sonicated cell can be obtained by solving a wave equation. For harmonic excitation, the wave equation is simplified to the Helmholtz equation, which is solved in COMSOL using the pressure acoustics module. In COMSOL the attenuation of the acoustic wave can be incorporated by assigning an attenuation coefficient, α, to the imaginary part of the wave number. In this study, the following formula is used to calculate the attenuation coefficient for water [6]:

$$\frac{\alpha}{f^2} = 25\times10^{-15} \quad (\text{Np s}^2/\text{m}) \tag{2}$$

in which f is the frequency of the ultrasound.

Table 1 The first resonance frequency and displacement amplitudes at different locations on the transducer end faces (V_e =50 V)

	Simulations	Experiments
First resonance frequency (kHz)	19.89	19.29
Displacement amplitude at top surface of the transducer (μm)	2.45	2.05
Displacement amplitude at centre of the horn tip (μm)	2.73	2.45
Displacement amplitude at perimeter of the horn tip (μm)	2.53	2.10

The computational domain of the cell is decomposed by triangular acoustic elements. It is important that the sizes of the elements must be small enough (at least 0.2 times the wavelength) to accurately resolve the wave pattern. The total number of elements is approximately 56000. The boundary conditions for all the surfaces in contact with air are set as traction-free. Dynamic coupling conditions between the structures and water are set at the boundaries of the wetted surfaces of the horn and of the vessel in the following ways:

1. For the structure, a distributed loading from the acoustic pressure in the water is assigned to the interfaces.
2. For the boundaries of the water, the normal component of the pressure gradient induced by structural vibration is fed back by setting the normal acceleration identical to that of the structure surface.

To verify the correctness of the coupling, effects of the cell water height and the distance from the horn tip to the cell bottom on the resonance frequency of the whole system are examined experimentally under the condition of a very low

ultrasonic intensity (without cavitation inception). The experimental setup is as shown in Figure 1. Experimental results are compared with the numerical simulations as shown in Tables 2 and 3. The differences between the simulations and experiments are less than 2.5%. Note that the experimental resonance frequency is determined by monitoring the vibration amplitude at the top surface of the transducer and the input electrical power. Both are found to reach maximum values when the system is in resonance.

Table 2 Effects of cell water height on the resonance frequency of the reactor (R=90 mm, h=143 mm). The driving voltage V_e =30 V results in a radiating intensity of about 0.04W/cm^2.

Liquid height in cell, H (mm)	Simulated resonance frequency (kHz)	Experimental resonance frequency (kHz)
148	19.86	19.41
153	19.85	19.39
158	19.83	19.38
163	19.82	19.36

Table 3 Effects of the distance of the horn tip to cell bottom on the resonance frequency of the reactor (R=90 mm, H=163 mm, V_e =30 V)

Distance from horn tip to cell bottom, h (mm)	Simulated resonance frequency (kHz)	Experimental resonance frequency (kHz)
143	19.82	19.36
148	19.74	19.26
153	19.63	19.17
158	19.50	19.06

RESONANT SONOCHEMICAL REACTOR FOR GENERATION OF CAVITATION FIELD

The major problem of the existing sonochemical reactors is that the efficient bandwidth of the transducer is in general quite small. For the Langevin-type piezoelectric transducer, the vibration vanishes fast as the driving frequency deviates from the resonance frequency (see, for example, Figure 2a). Even though there exist many possible resonance frequencies for a particular cell, the pressure field within the cell will be of low intensity if the transducer efficiency is low at these particular frequencies. Therefore, the key point is to design a cell which has an appropriate mode close to the resonance frequency of the transducer.

Also it should be bear in mind that once cavitation bubbles are presented in the cell, the acoustic characteristics (sonic speed, attenuation, modal nature, etc.) of the medium are changed. Indeed, Birkin et al. [3] found that the resonance frequency and the modal pattern of a cavitating cylindrical reactor are so sensitive that a 1 kHz-resolution of the driving frequency must be employed in their study. Furthermore, the multiple scattering produced by the bubbles must contribute directly to the sound distribution in the cell. Analysis of these effects is very complicated and is beyond the scope of this work.

In this section results from the FEM simulation are used as useful guidelines to design the optimal cell geometry of the sonochemical reactor. The aim is to realize a horn-type reactor which can generate a considerable volume of cavitation away from the horn tip only using a small irradiating intensity and specific power density. Several resonance modes are first found numerically by using different cell geometries. The theoretical cell geometry is then used as a referral for searching the optimal cell geometry and the corresponding cavitation mode in experiments.

Figure 4 illustrates a comparison of one of the resonance modes obtained numerically with the corresponding experimental cavitation field. The modal frequency and cell geometry between the simulation and the experiment are slightly different. The experimental irradiating intensity and specific energy density are only 0.135 W/cm^2 and 9.6×10^{-4} W/cm^3, respectively. The highest pressure and the cavitation bubbles are very close to the horn tip. Therefore, it is not an ideal mode for sonochemical applications since severe erosion will occur at the horn surface.

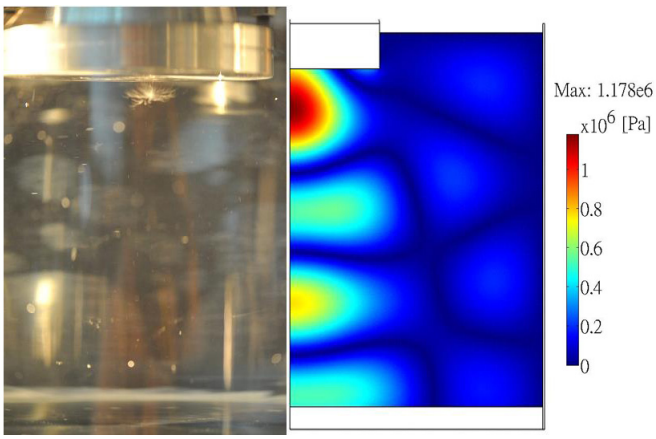

Figure 4 Left: photograph of resonance cavitation field in the experimental water cell (R=144 mm, H=170 mm, h=160 mm, V_e=85 V and I_e=250 mA, P_e=10.625 W, f_r=19.16 kHz). Right: simulated distribution of pressure amplitude in the resonance cell (R=141 mm, H=165 mm, h=149 mm, f_r=19.84 kHz).

By using the same cell vessel but adjusting the water height and the distance from the horn tip to the bottom of the cell, a

cavitation field with standing wave pattern is observed experimentally, as depicted in Figure 5. The distance between the cavitation layers is approximately half-wavelength (77 mm) of the ultrasound. The locations of these layers correspond to the antinodal planes of pressure as demonstrated by the simulation. The irradiating intensity and the specific energy density in the experiment are respectively 0.189 W/cm^2 and 12.5×10^{-4} W/cm^3.

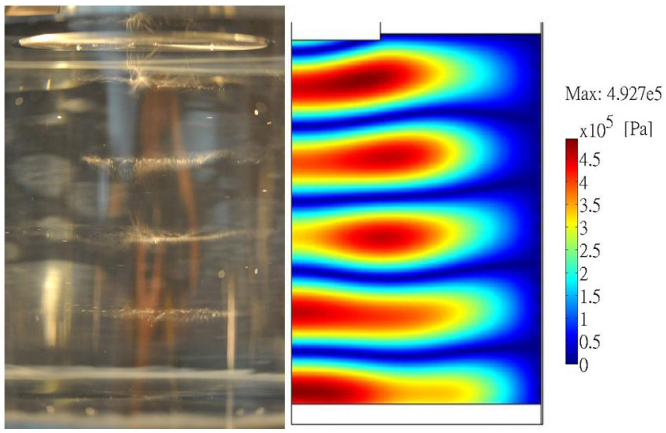

Figure 5 Left: photograph of resonance cavitation field in the experimental water cell (R=144 mm, H=182 mm, h=179 mm, V_e=85 V and I_e=350 mA, P_e=14.875 W, f_r=19.37 kHz). Right: simulated distribution of pressure amplitude in the resonance cell (R=142 mm, H=181 mm, h=178 mm, f_r=19.82 kHz).

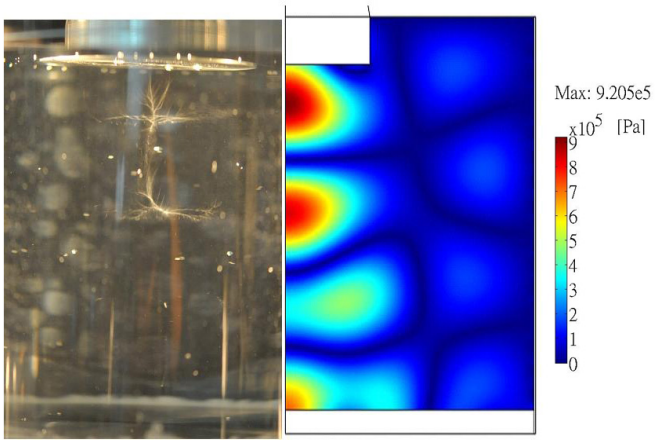

Figure 6 Left: photograph of resonance cavitation field in the experimental water cell (R=141 mm, H=161 mm, h=159 mm, V_e=85 V and I_e=250 mA, P_e=10.625 W, f_r=19.34 kHz). Right: simulated distribution of pressure amplitude in the resonance cell (R=147 mm, H=165 mm, h=145 mm, f_r=19.88 kHz).

Figure 6 shows a different modal pattern observed both in the simulation and in the experiment. The cavitation structure is composed of two layer-halos connected with a large amount of vertical streamers. It is noted that no bubbles attached on the radiating surface. The resonance mode shown in Figure 7 is obtained by using a cell geometry slightly different from that in Figure 6. A cone-like bubble structure combined with a horizontal cavitating layer are formed a little above the cell centre. Moussatov et al. [7] reported that, by using a 20.7 kHz cylindrical sonotrode of diameter 120 mm in water, a cone-like bubble structure attached on the radiating surface was formed when the irradiating intensity is greater than 3 W/cm^2. The cone-shape structure shown in Figure 7 is very similar to that observed by Moussatov et al. [7] except that it is located at a distance from horn surface and can be produced by using a very low irradiating intensity (0.119 W/cm^2).

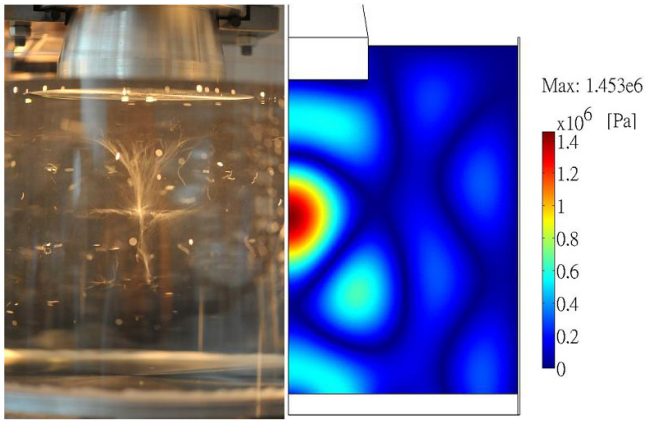

Figure 7 Left: photograph of resonance cavitation field in the experimental water cell (R=142.5 mm, H=159 mm, h=157 mm, V_e=85 V and I_e=220 mA, P_e=9.350 W, f_r=19.37 kHz). Right: simulated distribution of pressure amplitude in the resonance cell (R=144 mm, H=165 mm, h=149 mm, f_r=19.84 kHz).

CONCLUDING REMARKS

The horn-type sonochemical reactor has the advantage that the ultrasonic intensity irradiated by the transducer is directly related to the vibration amplitude of the horn tip. This can be precisely controlled by regulating the power input to the transducer. Most commercial sonochemical systems are designed only based on the electrical matching of the transducer to the amplifier. Although this guarantees a high efficiency of energy transfer to the transducer, it does not necessarily correspond to a high efficiency of energy transfer to sonochemical reactions. A large part of the irradiating energy can be consumed directly into heat by dissipation and is not associated with sonochemical effects.

In the present study, we have demonstrated that all the components of the reactor must be coupled together in analysis.

The reactor can behave as an efficient resonator under appropriate cell geometry. Experimentally it is shown that several optimal cell geometries can be realized under the limitation of narrow-bandwidth characteristics of the transducer. A large volume of cavitation bubbles is generated at the antinodal surfaces of the resonant pressure field by applying a very small irradiating intensity and specific power density. These results show the possibility of efficiently scaling up the horn-type sonochemical reactor without the drawback of cavitation erosion.

ACKNOWLEDGMENTS

The authors are grateful to the financial support from the National Science Council, Taiwan under contract No. NSC 97-2221-E-006-226.

REFERENCES

[1] Gogate, P.R., and Pandit, A.B., 2004, "Sonochemical Reactors: Scale Up Aspects," Ultrasonics Sonochemistry, **11**, pp. 105-117.

[2] Birkin, P.R., Leighton, T.G., Power, J.F., Simpson, M.D., Vincotte, A.M.L., and Joseph, P.F., 2003, "Experimental and Theoretical Characterization of Sonochemical Cells. Part 1. Cylindrical Reactors and Their Use to Calculate the Speed of Sound in Aqueous Solutions," J. Phys. Chem. A, **107**, pp. 306-320.

[3] Birkin, P.R., Power, J.F., Vincotte, A.M.L., Leighton, T.G., 2003, "A 1 kHz Resolution Frequency Study of a Variety of Sonochemical Processes," Phys. Chem. Chem. Phys., **5**, pp. 4170-4174.

[4] Klíma, J., Frias-Ferrer, A., González-García, J., Ludvík, J., Sáez V., and Iniesta, J., 2007, "Optimisation of 20 kHz Sonoreactor Geometry on the Basis of Numerical Simulation of Local Ultrasonic Intensity and Qualitative Comparison with Experimental Results," Ultrasonics Sonochemistry, **14**, pp. 19-28.

[5] Liu, M,, and Gorman, D.G., 1995, "Formulation of Rayleigh Damping and its Extension," Computers & Structures, **57**, pp. 277-285.

[6] Kinsler, L.E., Frey, A.R., Coppens, A.B., and Sanders, J.V., 1982, *Fundamentals of Acoustics*, 3rd ed., John Wiley & Sons.

[7] Moussatov, A., Granger, C., and Dubus, B., 2003, "Cone-like Bubble Formation in Ultrasonic Cavitation Field," Ultrasonics Sonochemistry, **10**, pp. 191-195.